

See discussions, stats, and author profiles for this publication at: <https://www.researchgate.net/publication/223970168>

Rational Design and Synthesis of Optimized Glycoclusters for Multivalent Lectin–Carbohydrate Interactions: Influence of the Linker Arm

ARTICLE *in* CHEMISTRY - A EUROPEAN JOURNAL · MAY 2012

Impact Factor: 5.73 · DOI: 10.1002/chem.201200010 · Source: PubMed

CITATIONS

28

READS

77

6 AUTHORS, INCLUDING:



Praly Jean

Claude Bernard University Lyon 1

115 PUBLICATIONS 1,836 CITATIONS

SEE PROFILE



Susan E Matthews

University of East Anglia

55 PUBLICATIONS 1,636 CITATIONS

SEE PROFILE



Michaela Wimmerová

Masaryk University

81 PUBLICATIONS 1,736 CITATIONS

SEE PROFILE



Anne Imberty

French National Centre for Scientific Resea...

361 PUBLICATIONS 10,342 CITATIONS

SEE PROFILE

DOI: 10.1002/chem.201200010

Rational Design and Synthesis of Optimized Glycoclusters for Multivalent Lectin–Carbohydrate Interactions: Influence of the Linker Arm

Samy Cecioni,^[a, b] Jean-Pierre Praly,^[a] Susan E. Matthews,^[c] Michaela Wimmerová,^[d]
 Anne Imberty,^{*[b]} and Sébastien Vidal^{*[a]}

Abstract: The design of multivalent glycoclusters requires the conjugation of biologically relevant carbohydrate epitopes functionalized with linker arms to multivalent core scaffolds. The multigram-scale syntheses of three structurally modified triethyleneglycol analogues that incorporate amide moiety(ies) and/or a phenyl ring offer convenient access to a series of carbohydrate probes with different water solubilities and rigidities. Evaluation of flexibility and determination of preferred conformations were performed

by conformational analysis. Conjugation of the azido-functionalized carbohydrates with tetra-propargylated core scaffolds afforded a library of 18 tetra-valent glycoclusters, in high yields, by Cu^I-catalyzed azide–alkyne cycloaddition (CuAAC). The compounds were evaluated for their ability to bind to PA-IL (the LecA lectin from the op-

portunistic pathogen *Pseudomonas aeruginosa*). Biochemical evaluation through inhibition of hemagglutination assays (HIA), enzyme-linked lectin assays (ELLA), surface plasmon resonance (SPR), and isothermal titration microcalorimetry (ITC) revealed improved and unprecedented affinities for one of the monovalent probes ($K_d = 5.8 \mu\text{M}$) and also for a number of the tetravalent compounds that provide several new nanomolar ligands for this tetrameric lectin.

Keywords: carbohydrates • click chemistry • glycoclusters • lectin • multivalency

Introduction

Carbohydrate–lectin interactions^[1–6] play a prominent role in various biological processes such as fertilization, cell–cell communication, viral and bacterial infection, cancer metastasis, and inflammation. The biomolecular interactions involved at the monovalent level between a carbohydrate and its specific lectin are usually in the millimolar range.^[3] Nature uses the so-called “cluster glycoside effect”^[7,8] through multivalent interactions with multiple copies of carbohydrate epitopes, lectins, or both to reach higher affinities and more specific biomolecular interactions. The concept of multivalency^[9–12] has therefore emerged as a powerful approach in both glycochemistry and glycobiology to design potent lectin ligands to prevent viral or bacterial infection for instance through anti-adhesive strategies.^[13,14] Nevertheless, the precise mode of action of such multivalent glycoconjugates is still not completely understood both at the biomolecular and biological level. The thermodynamics of such multivalent interactions is highly challenging and important contributions have been made over the past decades using isothermal titration microcalorimetry^[15,16] (ITC) among other bioanalytical techniques.^[17]


Bacterial lectins are involved in the early stages of infection, and competing with their binding to human glycoconjugates is an appealing alternative or complement to antibiotic treatment.^[13,18] PA-IL (LecA) from *Pseudomonas aeruginosa* is a tetrameric calcium-dependent lectin with specificity for α -galactose-terminated oligosaccharides^[19–21] and for β -galactosides with hydrophobic aglycon.^[22] The inhibition of PA-

[a] Dr. S. Cecioni, Dr. J.-P. Praly, Dr. S. Vidal
 Institut de Chimie et Biochimie
 Moléculaires et Supramoléculaires
 Laboratoire de Chimie Organique 2
 Glycochimie, UMR 5246, CNRS,
 Université Claude Bernard Lyon 1
 43 Boulevard du 11 Novembre 1918
 69622 Villeurbanne (France)
 Fax: (+33) 472-432-752
 E-mail: sebastien.vidal@univ-lyon1.fr

[b] Dr. S. Cecioni, Dr. A. Imberty
 Centre de Recherche sur les
 Macromolécules Végétales (CNRS)
 affiliated with Université Joseph Fourier
 Grenoble and ICMG
 BP 53, 38041 Grenoble (France)

[c] Dr. S. E. Matthews
 School of Pharmacy
 University of East Anglia
 Norwich, NR4 7TJ (UK)

[d] Dr. M. Wimmerová
 Central European Institute of Technology
 Masaryk University
 62500 Brno (Czech Republic)

 Supporting information for this article is available on the WWW under <http://dx.doi.org/10.1002/chem.201200010>. It includes experimental procedures for all new compounds, SPR sensorgrams and ITC data for monovalent and multivalent ligands, molecular modeling information, characterization with copies of ¹H and ¹³C NMR spectra for all new compounds, and crystallographic data for compound **1e**.

IL by simple monosaccharides was shown to be efficient for decreasing the population of *P. aeruginosa* in infected lungs for both mice models and human patients with cystic fibrosis.^[23,24] To obtain highly efficient competitors, we and others have synthesized multivalent galactosylated glycoclusters based on dendrimers,^[22,25] calix[4]arenes,^[26] calix[6]arenes,^[27] fullerenes,^[28,29] resorcin[4]arenes,^[30] porphyrins,^[27] β -peptides,^[27] and poly(phenylacetylene).^[31] Among these molecules, the 1,3-alternate conformer of calix[4]arene demonstrated a dramatic increase in affinity, and a chelate aggregative binding mode was suggested on the basis of molecular modeling.^[26] Recently, this hypothesis was further supported by the observation of well-defined nanometric fibers of lectin/glycocluster complexes through atomic force microscopy (AFM) investigations.^[32] Tetravalent-based scaffolds therefore appear to be particularly appropriate for high-affinity binding to PA-IL.

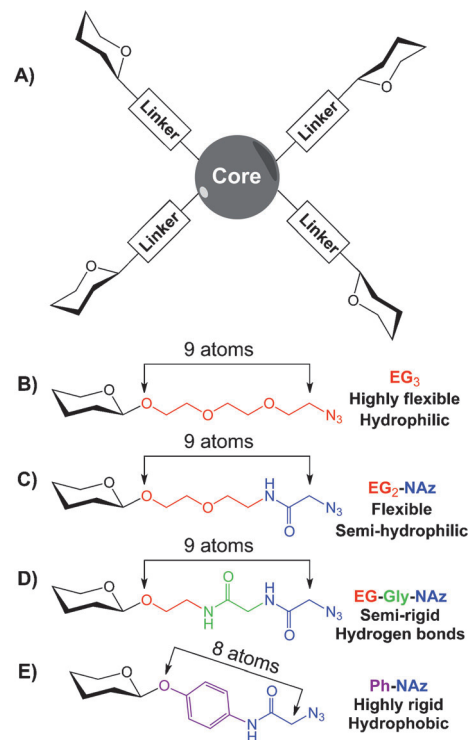
As a rational continuation of the project, second-generation tetravalent glycoclusters are reported herein, with the aim of optimizing the thermodynamic contributions, that is, enthalpy and entropy of binding, in the design of new optimized linkers. The design of high-affinity ligands for lectins requires the best possible match between valency and topological display of the carbohydrate epitopes that surround the multivalent core scaffold. Both of these parameters have been extensively examined in the literature,^[10–12] and the influence of the linker arm that connects the carbohydrate to the central core unit has also been previously addressed.^[33–43] The design of spacer arms that present different rigidities with similar lengths would provide the basis for a careful analysis of the parameters that govern multivalent carbohydrate–lectin interactions. Gains in enthalpy would arise from modifications of the structure of the carbohydrate epitope through additional stabilizing contacts, but increased affinities for lectins can also be obtained with more rigid linker arms, which decrease the entropic cost upon binding.

Oligo(ethyleneglycol)s are typical spacer arms used for the design of multivalent glycoconjugates; they have the advantage of being water soluble, of various lengths, and with an alcohol moiety that can be either easily derivatized to alternative functional groups or even directly involved in a glycosidic bond for connection to the carbohydrate epitope. Triethyleneglycol (EG₃) is a very common member of this family, and numerous examples have been previously described in the literature.^[26,44–50] This linker arm is easy to introduce through glycosylation but also provides improved water solubility for the resulting multivalent ligands synthesized. The sp³ hybridization of carbon and oxygen atoms along its chain provides a high freedom of movement for the terminal carbohydrate epitopes.

Linker arms with sp²-hybridized atoms in a chain analogous to EG₃ in terms of length can be used to obtain glycoclusters that present more rigidity than the parent EG₃-based structures. Such glycoconjugates would provide a relative entropic gain and therefore better binding properties towards the lectin. Nevertheless, the introduction of rigidifying motifs in the linker arm should be accurately balanced since

a too rigid linker may not allow the second epitope to reach its binding pocket on the multivalent lectin in a chelate binding mode.

The general formula of the glycoclusters presented here (Scheme 1A) is based on a multivalent central core scaffold with an EG₃ spacer arm as previously described^[26]



Scheme 1. Structure of the designed linker arms and their respective characteristics. EG = ethyleneglycol, NAz = *N*-azidoacetyl, Gly = glycine, Ph = phenyl.

(Scheme 1B). The introduction of one amide or two amide moieties into the EG₃ chain of the linker arm (Scheme 1B and C) should provide more rigid chains.^[51] The C=O and NH groups of the amide moieties could also interact with the side chain of the lectin polypeptide, thus leading to potentially more favorable enthalpic contributions. The introduction of a phenyl aromatic group (Scheme 1E) modifies the general structure of an EG₃-type chain and also its length. This hydrophobic moiety was selected based on experimental results that demonstrate that a strong gain in affinity for PA-IL can be obtained with a β -galactoside that contains an aromatic aglycon.^[22,52]

Results and Discussion

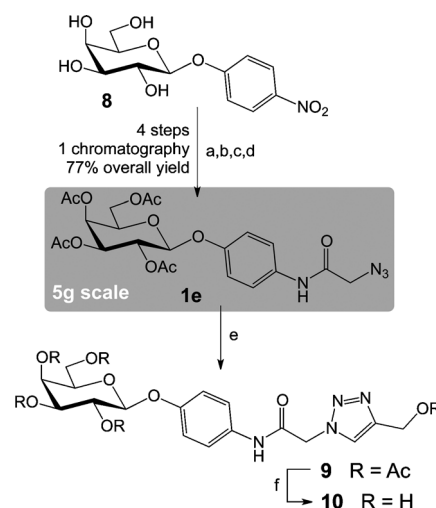
Synthesis: The different carbohydrate probes were synthesized on a multigram scale in a limited number of steps. We recently reported a high-yield glycosylation protocol that started from 1,2,3,4,6-penta-*O*-acetyl- β -D-galactopyranose under activation with tin(IV) and silver(I) salts.^[53,54] This re-

visited protocol affords the desired glycosides in high yields, complete stereoselectivity, and short reaction times, but also starts from a nonactivated galactose derivative in comparison to glycosyl bromides or trichloroacetimidates. This efficient glycosylation methodology has been applied to the preparation of β -D-galactopyranoside **1b** from the commercially available chlorinated diethyleneglycol and subsequent azidation (Scheme 2). The azidoacetyl group was then introduced by reduction, acylation, and azidation to afford **1c** after a single chromatographic purification step. To observe an unbiased effect of the multivalent presentation of carbohydrate epitopes, it was of prime importance to prepare suitable monovalent references that included the epitope and the whole linker arm. Therefore, the Cu^I-catalyzed azide-alkyne cycloaddition^[55–57] (CuAAC), under microwave irradiation, of **1c** with propargyl acetate afforded the desired 1,4-substituted 1,2,3-triazole **2** in a short reaction time. The subsequent solvolysis of the ester groups afforded the hydroxylated derivative **3**.

Similarly, the glycosylation of 2-chloroethanol and subsequent azidation afforded **4**, which was then reduced to the amine. The crude intermediate was treated with *N*-chloroacetyl glycine under *N*-hydroxybenzotriazole/1-ethyl-3-(3-dimethylaminopropyl) (HOBt/EDCI) activation to obtain **5**, which was then converted to the corresponding azide **1d**. CuAAC of **1d** with propargyl acetate afforded the acetylated cycloadduct **6**, and deprotection of the acetate groups yielded the desired hydroxylated galactoside **7**.

The commercially available 4-nitrophenyl β -D-galactopyranoside **8** was converted into the azido-functionalized derivative **1e** in four steps with only one chromatographic purification and in 77% overall yield (Scheme 3). Similarly, the CuAAC with propargyl acetate afforded **9**, and the hydroxylated derivative **10** was then obtained by solvolysis of the ester-protecting groups.

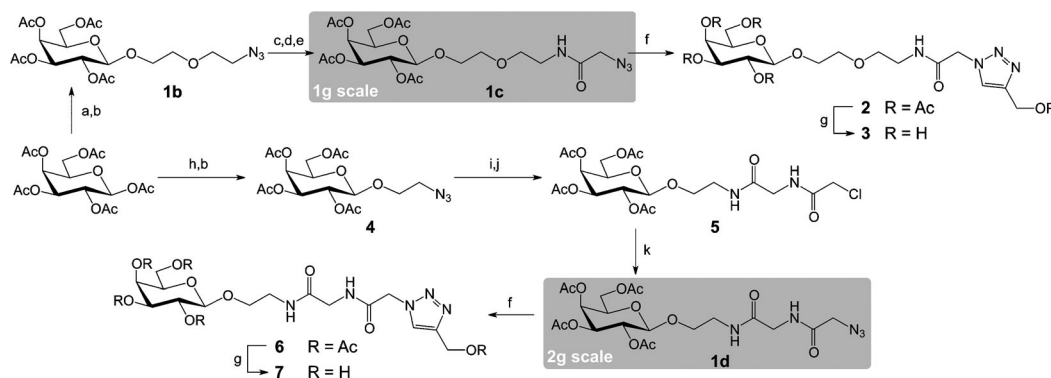
Single crystals suitable for X-ray crystallography were obtained by crystallization of **1e**, and analysis of the data collected displayed the expected *Z* configuration of the amide



Scheme 3. Syntheses of the aromatic monovalent probe. Reagents and conditions: a) Ac₂O, C₅H₅N, 4-dimethylaminopyridine (DMAP), RT, 16 h; b) H₂, Pd/C 10%, CH₂Cl₂, RT, 16 h; c) BrCH₂COBr, Et₃N, CH₂Cl₂, RT, 2 h; d) NaN₃, *n*Bu₄NI, DMF, 50°C, 16 h, 74% over four steps; e) propargyl acetate, CuI, *i*Pr₂NEt, DMF, 110°C, microwaves, 15 min, 98%; and f) MeOH, H₂O, Et₃N, RT, 16 h, 95%.

bond along with an overall planar geometry of the Ph–NAz linker arm (Figure 1). The three-dimensional crystal packing is achieved through weak C–H...O intermolecular interactions. All bond lengths and angles are within the expected values. The aromatic ring is tilted between the benzene ring and the mean plane of the sugar cycle (through C1 and C4) with an angle of 34.8°. A distance of 10.8 Å was measured between the anomeric carbon atom and the terminal azido nitrogen atom.

With azido-functionalized precursors in hand, conjugations of the carbohydrate probes **1c**, **1d**, **1e**, or **1a**^[29] were then performed by CuAAC with several propargylated core scaffolds to afford acetylated glycoclusters (Scheme 4). The tetra-propargylated methyl glucoside **11g**^[58] was obtained by Williamson etherification of methyl α -D-glucopyranoside.



Scheme 2. Syntheses of the mono-amide and bis-amide derivatives. Reagents and conditions: a) HOCH₂CH₂OCH₂CH₂Cl, SnCl₄, CF₃CO₂Ag, CH₂Cl₂, RT, 2 h; b) NaN₃, *n*Bu₄NI, DMF, 85°C, 16 h, 57% for **1b** and 78% for **4** over two steps; c) H₂, Pd/C 10%, CH₂Cl₂, RT, 16 h; d) BrCH₂COBr, Et₃N, CH₂Cl₂, RT, 12 h; e) NaN₃, *n*Bu₄NI, DMF, 80°C, 16 h, 57% over three steps; f) propargyl acetate, CuI, *i*Pr₂NEt, DMF, 110°C, microwaves, 15 min, 72% for **2** and 99% for **6**; g) MeOH, H₂O, Et₃N, RT, 16 h, 94% for **3** and 78% for **7**; h) HOCH₂CH₂Cl, SnCl₄, CF₃CO₂Ag, CH₂Cl₂, RT, 2 h; i) H₂, Pd/C 10%, CH₂Cl₂, RT, 20 h; j) *N*-chloroacetyl glycine, EDCI, HOBt, CH₂Cl₂/DMF, RT, 16 h, 54% over two steps; and k) NaN₃, *n*Bu₄NI, DMF, 80°C, 16 h, 78%.

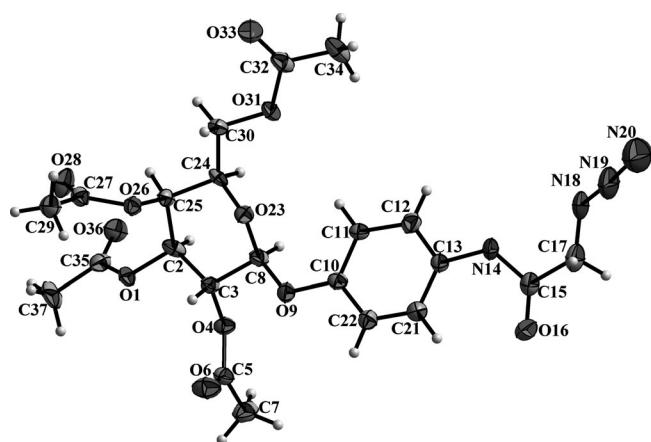


Figure 1. ORTEP view of the asymmetric unit of the unit cell of **1e** showing 30 % probability displacement ellipsoids.

The conjugations to prepare **12aG**, **12cG**, **12dG**, and **12eG** proceeded with modest yields (about 50 %) when considering the overall yield of the reaction but represented an average yield of 85 % per reactive site. Couplings of the glycosides with the tetra-propargylated Zn–porphyrin **11P**^[27,59] also proceeded smoothly under microwave activation with no exchange of the chelated metallic ion to yield acetylated glycoclusters **14aP**,^[27] **14dP**, and **14eP** in high yields. The synthesis of topoisomeric tetra-propargylated calix[4]arenes was previously described,^[26] and CuAAC coupling with azido-functionalized carbohydrates provided various conformers of tetravalent calix[4]arene-based glycoclusters. Thus, cone tetra-propargylated calix[4]arene **11C** yielded acetylated glycoclusters **16aC**,^[26] **16dC**, and **16eC**, whereas the 1,3-alternate conformer **11A** provided glycoclusters **18aA**,^[26] **18bA**, **18cA**, **18dA**, and **18eA** with high yields, and the partial cone conformer **11PC** afforded acetylated compounds **20aPC**, **20dPC**, and **20ePC**. These calixarene-based atropoisomers were stable during CuAAC conjugation under microwave irradiation since no modification of the conformation were observed by NMR spectroscopic analyses and characteristic ¹H signals were conserved for each conformation. The deprotection method for the solvolysis of the acetate groups by using MeOH/H₂O/Et₃N was carefully chosen because it creates byproducts that are easily eliminated under vacuum and therefore does not require purification of the final hydroxylated glycoclusters. All acetylated and hydroxylated glycoclusters were fully characterized by NMR spectroscopy (1D and 2D) and high-resolution mass spectrometry (HRMS).

Interaction of the monovalent references with PA-IL: To determine the influence and contribution of the spacer on the affinity for the studied lectin PA-IL, all monovalent references were assessed in the interaction study. In a first series of experiments (Table 1), the ability of monovalent probes to inhibit binding of PA-IL to glycosylated surfaces was evaluated by hemagglutination inhibition assays (HIA), enzyme-linked lectin assays (ELLA), and surface plasmon

Table 1. Biochemical evaluation of the monovalent probes for their binding to PA-IL.

| | Ligand | HIA MIC [μM] | ELLA IC ₅₀ [μM] | SPR IC ₅₀ [μM] |
|-----------|-----------------------------------|-----------------|-------------------------------|------------------------------|
| | β-D-GalOMe ^[a] | 5000 | 127.5 | n.d. ^[b] |
| 22 | GalEG ₃ ^[a] | 10000 | 220 | 63.5 |
| 3 | GalEG ₂ NAz | 10000 | 350 | 58.3 |
| 7 | GalEGGlyNAz | 2500 | 300 | 60 |
| 10 | GalPhNAz | 250 | 46 | 2.6 |

[a] Synthesized from the literature^[27] and see Scheme 5 for structural description. [b] n.d. = not determined.

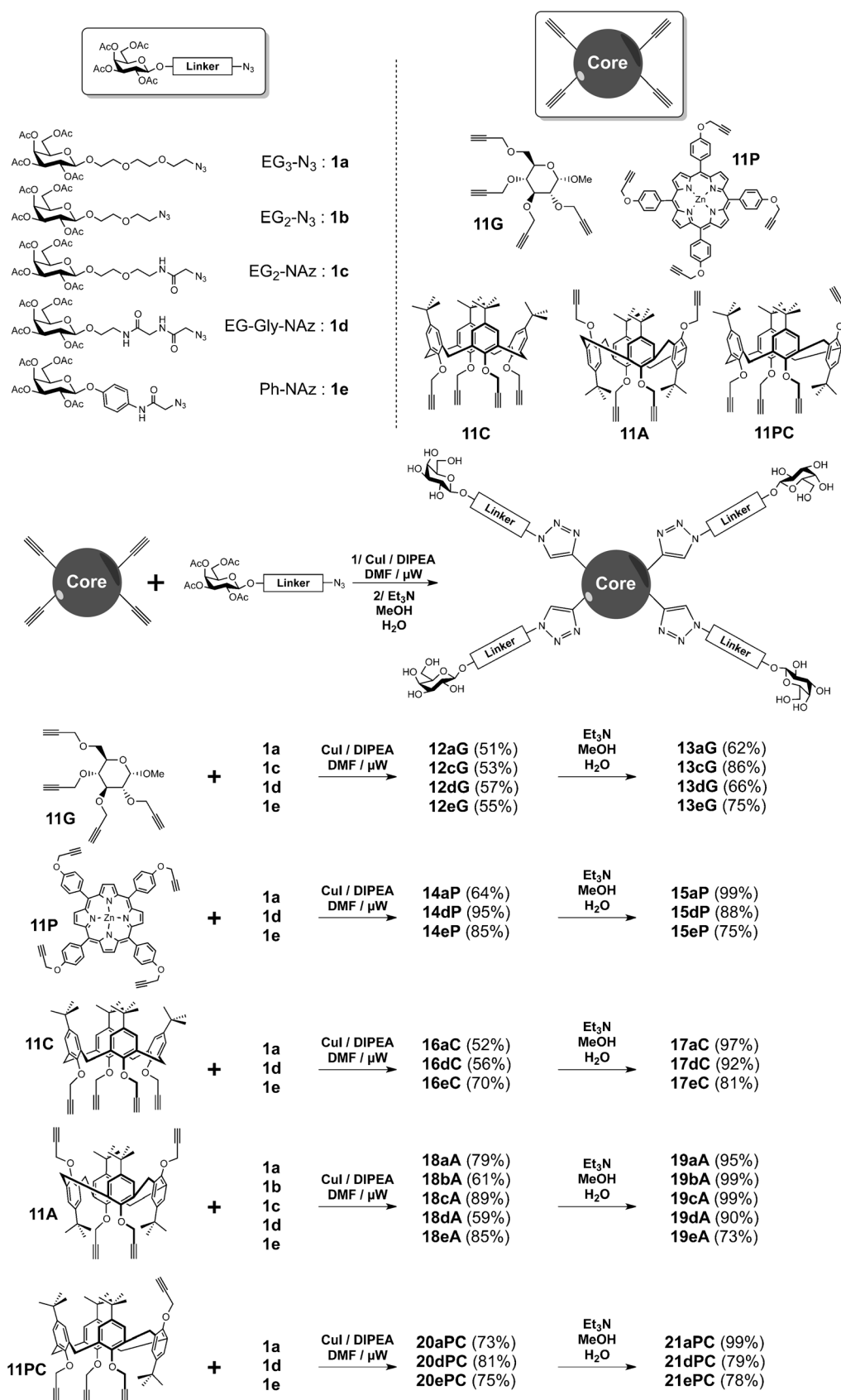
resonance (SPR). In the HIA assays, ligands **22**,^[26] **3**, and **7** that bore aliphatic linker arms displayed weak minimum inhibitory concentrations (MIC), whereas the *p*-amidophenyl-based ligand **10** demonstrated a significant improvement with submillimolar MIC.

Evaluation of IC₅₀ values (concentration that gives 50 % inhibition) by other biochemical techniques (ELLA and competitive SPR; Table 1) highlighted similar profiles with comparable inhibition potencies for aliphatic compounds **22**, **3**, and **7**, and strong improvement in the inhibition potency of the aromatic ligand **10** (Figure 2). These results were of great interest in evaluating the influence of different linker arms on the binding properties of multivalent glycoclusters. The linkers of molecules **22**, **3**, and **7** did not appear to strongly influence the binding of the monovalent probe, thereby indicating that the linker is not likely to interact with the surface. In contrast, the aromatic linker of **10** appeared to provide an optimized structure from the glycomimetic approach. We therefore had in hand linkers with very different properties, even at the monovalent compound level.

Further studies were undertaken by using isothermal titration microcalorimetry (ITC) to measure precisely the affinities between monovalent glycoclusters and PA-IL and to determine the enthalpy and entropy contributions of the binding energy. Compounds **22**, **3**, and **7** have submillimolar-range dissociation constant (*K*_D), and the titrations were conducted with an excess amount of ligand and fixed stoichiometry as recommended for low-affinity systems^[60] (see the figures in the Supporting Information). The higher-affinity aromatic ligand **10** provided a well-defined sigmoid during titration (Figure 3) with a stoichiometry value of 0.82, close to the value of *n* expected from structural data.

The introduction of one amide residue in **3** compared to **22** did not modify significantly the binding to PA-IL with *K*_D for the monovalent ligand **3** of 107 μM (Table 2). The introduction of a second amide motif was slightly more detrimental and resulted in a *K*_D value of 181 μM for compound **7**. Overall, the affinities of **22**, **3**, and **7** for PA-IL are in the same range. Titration of PA-IL with the aromatic ligand **10** yielded the determination of a *K*_D value of 5.8 μM, which is an unprecedented affinity for a monovalent glycomimetic toward this bacterial lectin.

When looking at the thermodynamic contributions, it can be noted that enthalpic contributions increase along with



Scheme 4. Syntheses of 18 glyoclusters with rigidified linker arms.

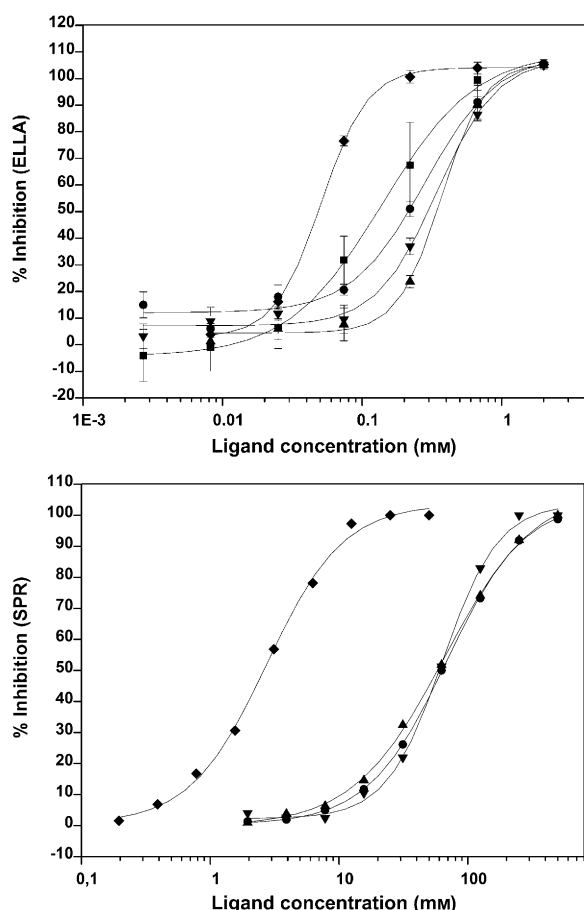


Figure 2. ELLA (top) and SPR (bottom) inhibition plots: ■) β -D-GalOMe, ●) **22**, ▲) **3**, ▼) **7**, ◆) **10**. Errors bars represent standard deviation over triplicates (ELLA only).

the hypothesized rigidity from compound **22** to ligands **3** and then **7**. This improvement in enthalpy could be explained by additional contacts between amido moieties of the linker arm and the lectin polypeptide backbone. Indeed, there is a 12 kJ mol^{-1} increase in enthalpy (ΔH) between ligands **22** and **3** and a further 15 kJ mol^{-1} rise between compounds **3** and **7**, which could account for one and then two additional N–H \cdots O hydrogen bonds. Meanwhile, entropic cost ($-T\Delta S$) increases by 12 kJ mol^{-1} between **22** and **3** and by 17 kJ mol^{-1} between **3** and **7**. Even though supplementary hydrogen bonds or an increase in water solvation could account for the increase in entropic cost, this behavior remains quite intriguing, as it is frequently assumed that rigidification of the structure would diminish the loss of entropy in the bound state.

The higher affinity of compound **10** relative to **22** is due to a much stronger enthalpy of binding (17 kJ mol^{-1} more than **22**) accompanied by a limited additional entropic cost (9 kJ mol^{-1}). The incorporation of an anomeric aromatic moiety is known to create additional hydrophobic contacts that result in higher desolvation of both ligand and receptor upon binding. This is in agreement with recent data that in-

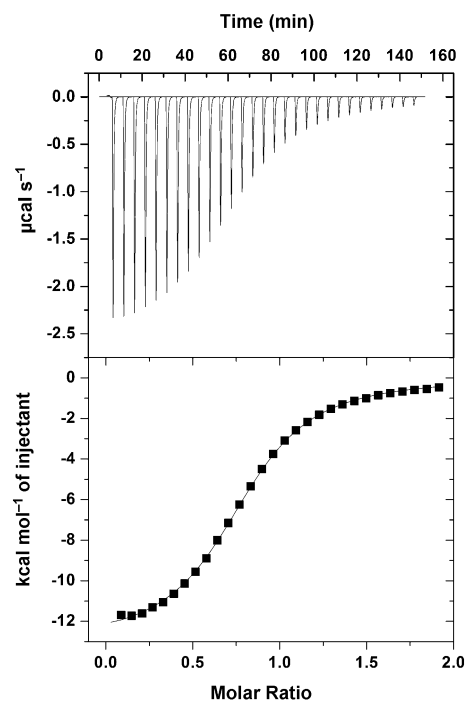


Figure 3. Raw ITC data (top) obtained by injections of **10** ($700 \mu\text{M}$) in a solution containing PA-IL ($82 \mu\text{M}$). Corresponding integrated titration curve (bottom).

Table 2. Isothermal titration microcalorimetry (ITC) for the monovalent probes and PA-IL.

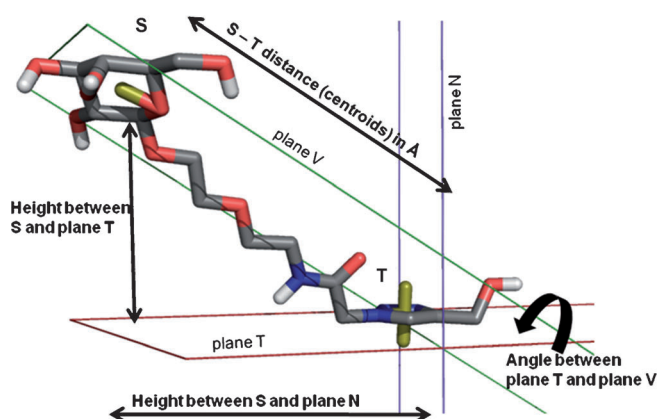
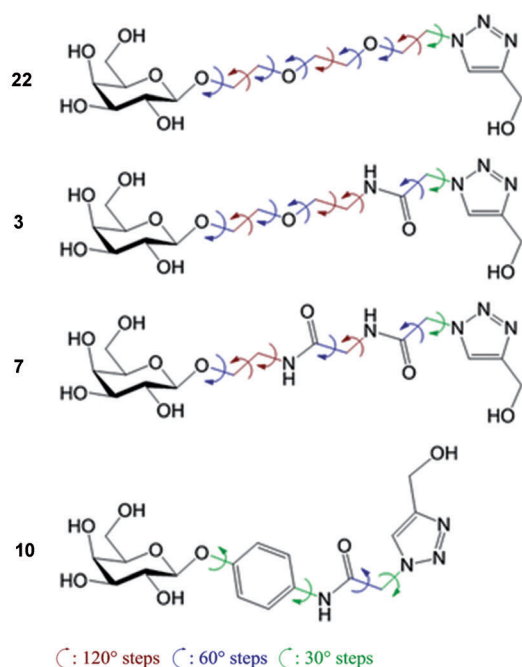
| Ligand | $n^{[a]}$ | $-\Delta H^{[b]}$ [kJ mol $^{-1}$] | $-T\Delta S$ [kJ mol $^{-1}$] | $K_D^{[b]}$ [μM] |
|---|------------------|--|-----------------------------------|----------------------------------|
| β -D-GalOMe ^[c,d] | 1 ^[e] | 39 | 15 | 70 |
| 22 GalEG ₃ ^[f] | 1 ^[e] | 36 ± 1 | 14 | 150 ± 1 |
| 3 GalEG ₂ NAz | 1 ^[e] | 48.8 ± 0.7 | 26 | 107 ± 7 |
| 7 GalEGGlyNAz | 1 ^[e] | 64 ± 11 | 43 | 181 ± 12 |
| 10 GalPhNAz | 0.81 ± 0.01 | 53 ± 2 | 23 | 5.8 ± 0.9 |

[a] Stoichiometry. [b] Standard deviation is given over 2 or 3 experiments. [c] Only one experiment performed. [d] Data from the literature.^[27] [e] Fitting with constant stoichiometry determined with *p*-nitrophenyl- β -D-galactopyranoside. [f] Data from the literature.^[26]

dicates that the aromatic ring interacts directly with the PA-IL protein surface in the proximity of the binding site.^[22]

Molecular modeling of linker flexibility: To further investigate the conformational freedom and geometry of the rigidified monovalent ligands, a molecular modeling procedure was developed based on previously described methodology.^[61] The ligands were built in silico; the rotatable bonds were defined as well as a set of geometrical descriptors for analyzing the key structural features of the monovalent ligands (Scheme 5).

Centroid S was defined by the galactose ring atoms and centroid T by the triazole ring atoms. Plane V was composed of centroids S and T and the endocyclic oxygen atom. Plane T was built on the three atoms of the triazole ring and



Scheme 5. Top: Definition of rotatable bonds and torsional increments during systematic conformational search. Bottom: Geometrical parameters measured for all conformations obtained from each ligands (e.g., ligand 3 presented here).

plane N by using an axis perpendicular to the centroid T and the C5 atom of the triazole ring.

For each ligand, a systematic search was performed in the conformational space defined by the rotatable bonds. All conformations with a relative energy cutoff of 20 kcal mol⁻¹ were analyzed. The geometrical properties were calculated by taking into account the probability of each conformation as a function of its relative energy according to Boltzmann equations [Eqs. (1) and (2)] in which p_i is the probability of existence of one given conformation, E_i is the energy of the conformation, and k is the Boltzmann constant. This calculation allowed us to plot the probability of existence of conformations as a function of the geometrical parameters (Figures 4, 5, and 6).

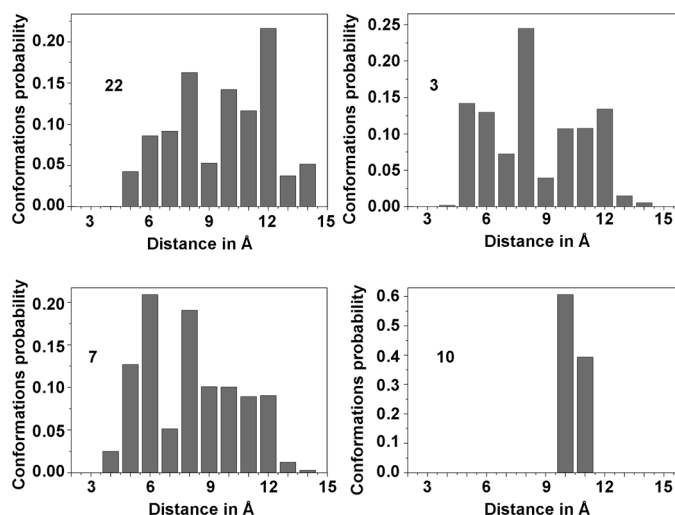


Figure 4. Modeled probability as a function of distance between S and T (centroids).

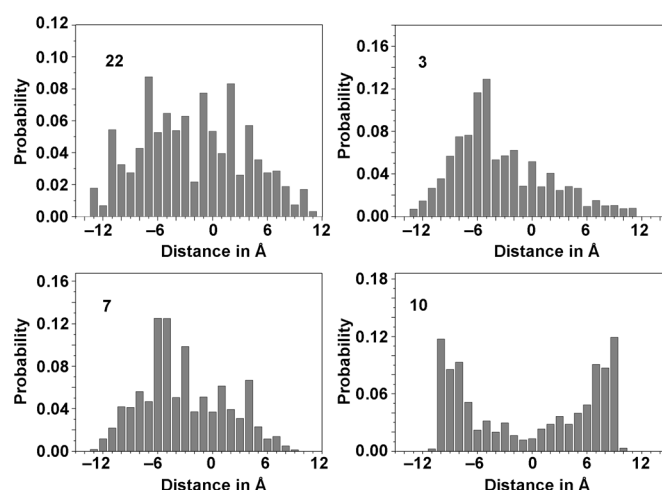


Figure 5. Modeled probability as a function of height between S and plane T.

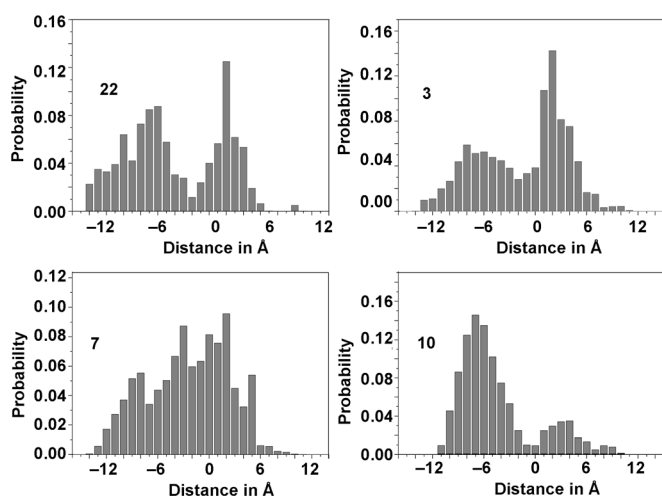


Figure 6. Modeled probability as a function of height between S and plane N.

$$p_i = \frac{e^{\left(\frac{-E_i}{kT}\right)}}{Q} \quad (1)$$

$$Q = \sum_i e^{\left(\frac{-E_i}{kT}\right)} \quad (2)$$

Using the energy-weighted values (Boltzmann probability), the distance between centroids S and T—that is, the elongation of the molecule—varies between 5 and 14 Å for monovalent ligands **22**, **3**, and **7** (Figure 4). Small differences are observed for the preferred shape with compound **22** being more elongated than the other two. In contrast, extension of compound **10** closely centered around a value of 10 Å.

The heights between centroid S and plane T or plane N also showed comparable behavior for ligands **22**, **3**, and **7** but with a slight preference for negative values (Figures 5 and 6). Positive and negative values indicate that the sugar could move to both sides of the planes without high energy penalties. For compound **10**, a distribution centered on two symmetric values of −10 and 9 Å was observed.

These results indicate a high flexibility for compounds **22**, **3**, and **7** with little difference between them, which stands in contradiction to the initial hypothesis for the chemical design of the second-generation ligands. On the other hand, ligand **10** clearly shows less flexibility and adopts a more restrained conformational behavior by populating a limited number of conformational families.

Evaluation of the second-generation glycoclusters (HIA, ELLA, and SPR): The second-generation glycoclusters proposed here have been synthesized based on previously described multivalent core scaffolds but with optimized linker arms. Their evaluation as ligands of PA-IL was achieved through a set of complementary bioanalytical techniques (HIA, ELLA, SPR, and ITC; Tables 3 and 4). An improvement value (β) of MIC or IC_{50} values was calculated versus the appropriate monovalent reference for each analytical technique.

Analysis of HIA results: During the HIA experiments, the first observation was the haemolysis caused by the PhNAz-based glycoclusters (**15eP**, **17eC**, **21ePC**, **19eA**, and **13eG**) that incorporated the aromatic linker arm. The β values obtained for the other glycoclusters were below 40, thereby highlighting a modest improvement of inhibition relative to the monovalent ligands. The glucose-cored glycoclusters **13aG** and **13dG** did not inhibit the agglutination of red blood cells by the lectin ($MIC > 2$ mM). Nevertheless, the GalEG₂NAz glycocluster **13cG** displayed an MIC value of 250 μ M. The number of amide bonds present in the linker arm therefore affects the inhibition properties towards PA-IL. The linker incorporating one amide bond can inhibit the lectin-promoted agglutination, whereas linkers that incorporate either none or two amide bonds are not active. The porphyrin-based glycoclusters **15aP** and **15dP** display β values of 159 and 2500, respectively, thus suggesting that these two

ligands are very efficient for the inhibition of agglutination of erythrocytes.

Analysis of ELLA results: All glycoclusters were soluble at the concentration required for the ELLA assays, except for **13eG**, that is, GalPhNAz conjugated to the tetra-propargylated glucose core (Figure 7). Modest β values ($9 < \beta < 57$) were obtained for GalPhNAz multivalent ligands (**15eP**, **17eC**, **21ePC**, and **19eA**), but these compounds are nevertheless efficient inhibitors since the monovalent GalPhNAz reference ligand **10** already displayed a low IC_{50} value of 46 μ M. As previously observed in the HIA evaluation, the porphyrin-based glycoclusters **15aP** and **15dP** displayed β values above 400 and displayed the best IC_{50} values for competitive binding to PA-IL as measured by ELLA.

Comparison of the β values obtained for the glucose-based glycoclusters **13aG**, **13cGm** and **13dG** illustrates the influence of the linker arm, as observed from the HIA data, and the mono-amide linker arm displayed the best binding towards PA-IL among this subfamily of three glycoclusters. Although the IC_{50} values measured in the ELLA assay for these glucose-based glycoclusters are very similar (2 to 9 μ M), the analysis of the β values demonstrates the influence of the linker arm on the improvement of binding properties relative to the monovalent ligands.

Analysis of SPR results: The GalPhNAz glycoclusters were not sufficiently soluble for SPR analyses. The IC_{50} values obtained for the glycoclusters are in the low to submicromolar range (Figure 7). The β values were rather modest and usually below 60. The best multivalent ligands identified by SPR analysis were the 1,3-alternate calixarene-based glycoclusters **19aA** and **19bA** with IC_{50} values of 0.5 and 0.6 μ M, respectively. The shorter EG₂-based linker was still capable of inhibiting the adhesion of PA-IL onto the galactose-coated gold surfaces used in the SPR experimental setup.

Although the rational design of the rigidified second-generation glycoclusters appeared promising, most of these multivalent ligands displayed potent binding properties for PA-IL with IC_{50} values in the low micromolar to nanomolar range as determined by ELLA and SPR. The improvement in binding due to multivalency was remarkable for some of the best molecules with β values of close to 100, but these remained comparable to the first-generation glycoclusters with EG₃-based linker arms.

Among the second-generation multivalent ligands, several structures displayed interesting inhibition features. The porphyrin-based glycocluster **15dP** demonstrated strong and promising potency both in HIA and ELLA. Calixarene-based glycoclusters **17dC**, **21dPC**, and **19dA** that bore the same bis-amide EGGlyNAz linker arm yielded interesting increases in the inhibition potency by ELLA. In HIA, these three multivalent ligands demonstrated smaller improvements.

Evaluation of the second-generation glycoclusters (ITC): ITC studies were then performed for the systematic analysis

Table 3. Biochemical evaluation of glycoclusters.

| Core | Linker | HIA | | ELLA | | SPR | |
|--|-----------------------------------|------------------------|---------------|------------------------------------|---------------|------------------------------------|---------------|
| | | MIC [μM] | $\beta^{[a]}$ | IC ₅₀ [μM] | $\beta^{[a]}$ | IC ₅₀ [μM] | $\beta^{[a]}$ |
| 15aP ^[b] 15dP 15eP | GalEG ₃ | 63 | 159 | 0.5 | 440 | 1.4 | 45 |
| | GalEGGlyNAz | 1 | 2500 | 0.7 | 429 | 1.6 | 37.5 |
| | GalPhNAz | haemol. ^[d] | – | 2 | 23 | n.s. ^[e] | – |
| 17aC ^[b] 17dC 17eC | GalEG ₃ | 290 | 34 | 42 | 5.2 | 2.5 | 29 |
| | GalEGGlyNAz | 250 | 10 | 21 | 14 | n.s. ^[e] | – |
| | GalPhNAz | haemol. ^[e] | – | 0.8 | 57 | n.s. ^[e] | – |
| 21aPC 21dPC 21ePC | GalEG ₃ | 500 | 20 | 46 | 4.8 | 1.7 | 42 |
| | GalEGGlyNAz | 250 | 10 | 7 | 43 | 1.1 | 54 |
| | GalPhNAz | haemol. ^[d] | – | 0.9 | 51 | n.s. ^[e] | – |
| 19aA ^[b] 19cA 19dA 19eA 19bA | GalEG ₃ | 500 | 20 | 36 | 6.1 | 0.5 | 144 |
| | GalEG ₃ NAz | 500 | 20 | 7 | 50 | 1.0 | 58 |
| | GalEGGlyNAz | 625 | 4 | 14 | 21 | 1.2 | 50 |
| | GalPhNAz | haemol. ^[d] | – | 5 | 9 | 0.8 | 3.5 |
| | GalEG ₂ ^[c] | > 2000 | – | 15 | 15 | 0.6 | 105 |
| 13aG 13cG 13dG 13eG | GalEG ₃ | > 2000 | – | 9 | 24 | 2.8 | 23 |
| | GalEG ₃ NAz | 250 | 40 | 2 | 175 | 1.9 | 31 |
| | GalEGGlyNAz | > 2000 | – | 4 | 75 | 1.7 | 35 |
| | GalPhNAz | haemol. ^[d] | – | n.s. ^[e] | – | n.s. ^[e] | – |

[a] Improvement in IC₅₀ relative to the appropriate monovalent reference for each linker arm. [b] Data from the literature.^[27] [c] Monovalent reference used for that glycocluster is compound **22**. [d] haemol. = visual observation of red-cell haemolysis. [e] n.s. = not soluble under the experimental conditions required, even in the presence of 5 % of DMSO.

of the binding of glycoclusters to PA-IL. Unfortunately, the issue of solubility was even more pronounced in the microcalorimetry experimental setup, and only the more soluble compounds could be tested (Table 3). Glycoclusters built with GalPhNAz (**15eP**, **17eC**, **21ePC**, **19eA**, and **13eG**) and ligands based on porphyrin (**15dP** and **15eP**) and on the cone conformer of calix[4]arene (**17dC** and **17eC**) were not soluble enough for ITC measurements.

Soluble glycoclusters evaluated by ITC displayed K_D values in the nanomolar range with correspondingly high β values ($\beta > 357$) (Table 4). The glycoclusters with glucose scaffold **13cG** and **13dG** bound less tightly to PA-IL with K_D values of 800 and 1720 nM. However, two situations should be distinguished. First, the GalEGGlyNAz-based

multivalent ligands **21dPC** and **19dA** displayed an increase in the binding stoichiometry (n) relative to the first-generation EG₃-based glycoclusters (**21aPC** and **19aA**). These data suggest that these rigidified structures were not able to interact simultaneously with four PA-IL monomers but rather between two or three monomers. This feature was accompanied by lower enthalpic gains and entropic costs. Changes in stoichiometry would imply different binding mechanisms and therefore the interpretation of the linker arm influence on the binding to PA-IL strictly based on the thermodynamic profiles would be less appropriate. The glucose-based glycocluster **13dG** displayed a higher stoichiometry than ligand **13cG**. The latter gave a K_D value of 0.8 μM

Table 4. Thermodynamic parameters of glycoclusters upon binding to PA-IL (ITC) ($T=298\text{ K}$). (See Table 3 for the structures of the cores and linkers.)

| | $n^{[a]}$ | $-\Delta H^{[b]}$ [kJ mol $^{-1}$] | $-T\Delta S$ [kJ mol $^{-1}$] | K_D [μM] $^{[b]}$ | $\beta^{[c]}$ |
|-----------------------|-----------------|--|-----------------------------------|-------------------------------------|---------------|
| 15aP $^{[e]}$ | 0.46 ± 0.04 | 60 ± 7 | 23 | 0.33 ± 0.06 | 451 |
| 15dP | | | not soluble | | |
| 15eP | | | not soluble | | |
| 17aC $^{[f]}$ | 0.33 ± 0.01 | 71 ± 6 | 34 | 0.4 ± 0.1 | 357 |
| 17dC | | | not soluble | | |
| 17eC | | | not soluble | | |
| 21aPC $^{[f]}$ | 0.26 ± 0.01 | 98 ± 9 | 60 | 0.200 ± 0.005 | 750 |
| 21dPC | 0.38 ± 0.01 | 78 ± 2 | 40 | 0.239 ± 0.003 | 753 |
| 21ePC | | | not soluble | | |
| 19aA $^{[f]}$ | 0.24 ± 0.03 | 104 ± 1 | 65 | 0.176 ± 0.006 | 852 |
| 19cA | 0.24 ± 0.02 | 158 ± 2 | 119 | 0.09 ± 0.02 | 1138 |
| 19dA | 0.39 ± 0.03 | 91 ± 2 | 53 | 0.20 ± 0.04 | 891 |
| 19eA | | | not soluble | | |
| 19bA | 0.20 ± 0.01 | 147 ± 2 | 110 | 0.25 ± 0.09 | 595 |
| 13aG | | | poor quality fit $^{[d]}$ | | |
| 13cG | 0.32 ± 0.01 | 129.4 ± 0.1 | 95 | 0.80 ± 0.02 | 225 |
| 13dG | 0.44 ± 0.05 | 102 ± 10 | 69 | 1.72 ± 0.5 | 106 |
| 13eG | | | not soluble | | |

[a] Stoichiometry. [b] Standard deviation is given over 2 or 3 experiments. [c] Improvement of affinity relative to the appropriate monovalent reference (linker arm). [d] Heat signal increased during first injections. [e] Data from the literature. $^{[27]}$ [f] Data from the literature. $^{[26]}$

that was two times lower but remained a ligand with an intermediate affinity for PA-IL.

The second situation includes the second-generation ligands that display a 1:4 binding stoichiometry ($n \approx 0.25$) to PA-IL monomers, thus indicating that all galactose residues are engaged in a lectin binding site. The core scaffold that resulted in higher affinity was the 1,3-alternate calix[4]arene. With a stoichiometry of 0.24 and a K_D value of 90 nM, ligand **19cA** (Figure 8) showed a significant rise in enthalpic contribution relative to first-generation ligand **19aA**. This increase must be related to the increase observed during the evaluation of the monovalent reference **3**. Interestingly, the entropic cost of **19cA** binding with PA-IL was also increased significantly but did not counterbalance the enthalpic gain as observed for other glycoclusters. The resulting improved affinity of 90 nM corresponds to a 1138-fold increase relative to its monovalent probe **3**.

Plotting relative potencies (β) versus β -GalOMe for each of the glycoclusters (Figure 9) highlighted that the partial cone and 1,3-alternate conformers of calix[4]arenes were the most efficient core scaffolds. Among them, the 1,3-alternate calix[4]arene that bore EG₂NAz linker **19cA** was about twice the potency of the second-best glycocluster **19aA**. Multivalent ligands based on the cone conformer of calix[4]arene or on the glucose scaffold displayed modest potencies independently of the structures of the linkers.

Optimization of the structure of the linker arms yielded the highest-affinity ligand **19cA** for this bacterial lectin. By changing the structure of the first-generation ligand **19aA** to the optimized glycocluster **19cA**, it provided a twofold increase in affinity towards PA-IL with only a subtle modifica-

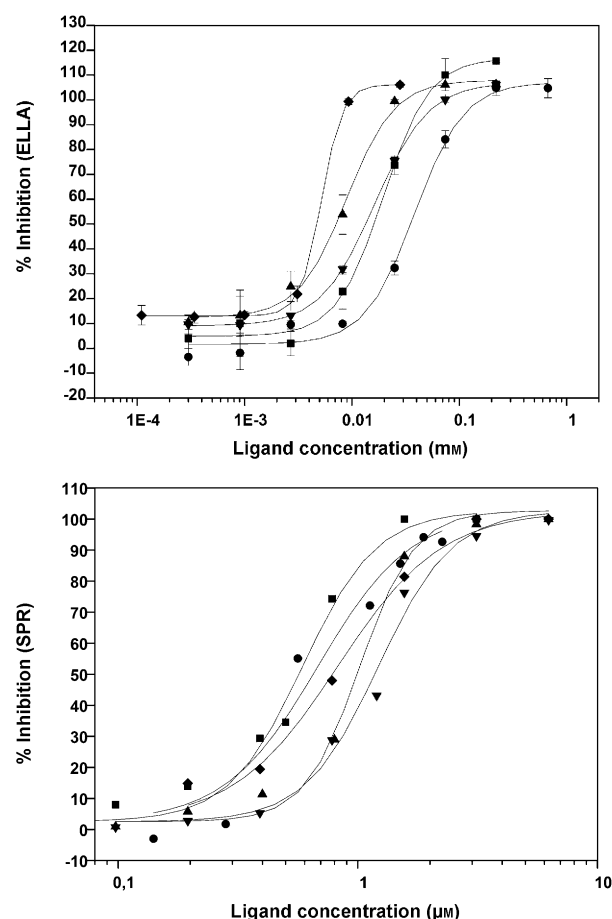


Figure 7. ELLA (top) and SPR (bottom) inhibition plots for the 1,3-alternate calixarene core scaffold: ● GalEG₃NAz **19aA**, ▲ GalEG₂NAz **19cA**, ▼ GalEGGlyNAz **19dA**, ◆ GalPhNAz **19eA**, ■ GalEG₂NAz **19bA**. Error bars represent standard deviation over triplicates.

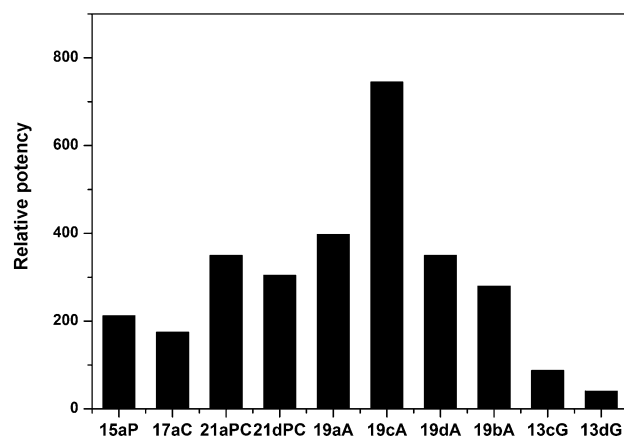


Figure 8. Column representation of the relative potency (β) of glycoclusters versus β -D-GalOMe against PA-IL as measured by ITC.

tion of its molecular structure. Introduction of a second amide moiety in the linker arm (i.e., glycocluster **19dA**) did not further improve the binding to PA-IL, but the observed

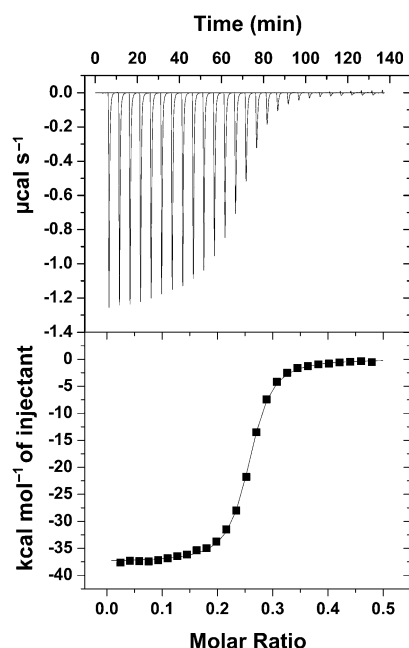


Figure 9. Raw ITC data (top) obtained by injecting a solution of **19cA** (120 μM) in a solution containing PA-IL (50 μM). Corresponding integrated titration curve (bottom).

K_D value was almost identical to the first-generation EG₃-based glycocluster **19aA**.

Finally, glycocluster **19bA** that bore the EG₂-based linker arm displayed only a slight affinity decrease for PA-IL with a K_D value of 250 nM. The free energy was composed of a stronger enthalpic contribution balanced by a higher entropic cost relative to the EG₂-based glycocluster **19aA**. The length of the linker arm could therefore be reduced to only two ethyleneglycol units while maintaining the simultaneous binding of four PA-IL monomers (n value of 0.20).

Plotting the enthalpic (ΔH) versus entropic ($-T\Delta S$) contributions measured by ITC for each multivalent glycocluster underlined the differences in the thermodynamic profiles related to the modifications of the ligand's chemical structure (Figure 10). Ligands **21dPC** and **19bA** have almost identical affinities (0.24 and 0.25 μM , respectively) but very different thermodynamic signatures. On the other hand, li-

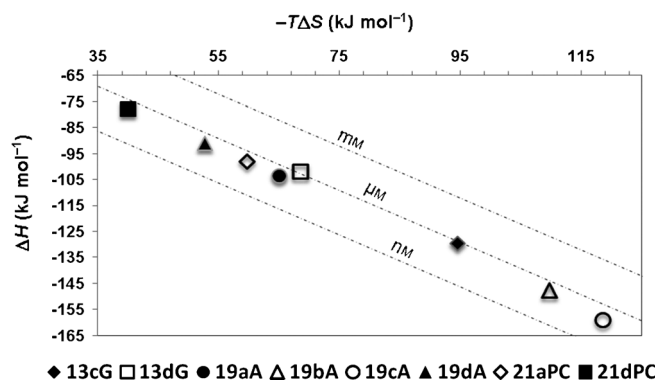


Figure 10. Enthalpic contribution related to entropic cost.

gands **21aPC** and **19dA** displayed the same K_D value and also a comparable thermodynamic profile. This type of graphical representation of the thermodynamic parameters of the biomolecular interaction provides a rapid and general overview of a large set of ligands to better identify the common binding features among them. At a given temperature (298 K), dissociation constant frontiers (from millimolar to micro- and nanomolar) illustrated the phenomenon sometimes referred as “enthalpy/entropy compensation.” This apparently linear correlation between enthalpy and entropy has been greatly discussed based on calorific capacities and solvent reorganization.^[62–65] The statistical significance of this phenomenon is still an area of investigation. The present studies illustrate that high affinity can be attained by using different strategies when designing multivalent glycoclusters.

Conclusion

In conclusion, a series of three azido-functionalized carbohydrate derivatives were prepared that incorporated analogues of triethyleneglycol as a linker arm. The selected structures incorporated one or two amide groups in a triethyleneglycol moiety for increased rigidity of the chain. A phenyl aromatic ring was also introduced and displayed unprecedentedly high affinity as a monovalent ligand of PA-IL. The synthetic routes are based on a combination of efficient and reliable glycosylation of peracetylated galactose, amide bond formation, and azidation. The azido-functionalized derivatives were then conjugated by azide–alkyne “click” chemistry methodology to either propargyl acetate to obtain a monovalent probe or to tetra-propargylated core scaffolds (porphyrin, three topologically isomeric calixarenes, and glucose) to afford the corresponding multivalent glycoclusters.

Binding towards PA-IL was investigated by using four bioanalytical techniques (HIA, ELLA, SPR, and ITC). Some variability was observed when comparing data from different techniques as observed previously by us and others.^[8,27,66] Differences appear in the scale of weak and strong ligands since ELLA and ITC appeared more powerful than SPR to discriminate between the most efficient ligands. Some differences are also observed in the order of efficiency. The reason for such differences was due to the different conditions of measurement (e.g., buffer, concentration) and the fact that different physical phenomena were measured (homogeneous solution versus surface adhesion). Nevertheless, the different methods used are in broad agreement and it was found that the higher efficiency of the 1,3-alternate calixarene represents the best galactose-presenting scaffold. Evaluation of the monovalent reference probes showed comparable inhibition potencies and affinities, except for the phenyl-containing compound, which is the highest-affinity ligand for PA-IL reported so far. The thermodynamic signatures displayed unexpected differences. Development of a molecular modeling approach provided

access to the geometrical parameters and flexibility of the monovalent ligands.

During the linker-arm optimization, solubility appeared to be a major issue for several synthesized multivalent glyco-clusters. This study clearly illustrates the complexity of predicting the influence of “rigidifying” the structure on the thermodynamic parameters. Indeed, significant improvement in the affinity of the second-generation rigidified multivalent ligands arose from a strong increase in enthalpic contribution rather than a decrease in entropic cost as initially hypothesized. Among rigidified glycoclusters, the shifts in stoichiometry highlighted variations in binding mechanisms, which made comparisons of thermodynamic patterns inappropriate.

The present study resulted in optimized molecular architectures as high-affinity ligands of PA-IL for potential therapeutic applications as anti-adhesive drugs that target *Pseudomonas aeruginosa* bacterial infections. When comparing those results with other multivalent ligands developed against this bacterial target,^[22,25] we have reported here very potent structures with the advantages of relative low molecular weights and straightforward synthetic strategies.

Experimental Section

Synthesis

Materials and methods: All reagents were commercial and used without further purification. Solvents were distilled over CaH_2 (CH_2Cl_2) or Mg/I_2 (MeOH). All the reactions were performed under an argon atmosphere. Reactions under microwave activation were performed using a Biotage Initiator system. NMR spectra were recorded at 293 K, unless otherwise stated, using a 400 MHz spectrometer. Shifts are referenced relative to deuterated solvent residual peaks. Complete signal assignments from 1D and 2D NMR spectroscopy were based on COSY, HSQC, and HMBC correlations. High-resolution (HR-ESI-QToF) mass spectra were recorded using a Bruker MicroToF-Q II XL spectrometer. Thin-layer chromatography (TLC) was carried out on aluminum sheets coated with silica gel 60 F_{254} (Merck). TLC plates were inspected by UV light ($\lambda = 254 \text{ nm}$) and developed by treatment with a mixture of 10% H_2SO_4 in $\text{EtOH}/\text{H}_2\text{O}$ (1:1 v/v) followed by heating. Silica gel column chromatography was performed with silica gel Si-60 (40–63 μm).

The numbering of molecules is written using a lower-case letter for the spacer arm used (**a–d**) but also a capital letter (**G** for glucose, **P** for porphyrin, **A** for the 1,3-alternate, **C** for the cone, and **PC** for the partial cone conformers of calixarenes) to provide some information about the general structure of the glycocluster.

General procedure for 1,3-dipolar cycloadditions (method A): The alkyne derivative, copper iodide, *N,N*-diisopropylethylamine (DIPEA), and azido derivative in DMF were introduced into a Biotage Initiator 2–5 mL vial. The solution was sonicated for 30 s. The vial was sealed with a septum cap and heated at 110 °C for 15 min under microwave irradiation (solvent absorption level: high). If the product was partially soluble in water, the crude mixture was concentrated and co-evaporated with toluene three times before flash chromatography. If the product was not soluble in water, the mixture was diluted with EtOAc (250 mL). The organic layer was washed with 150 mL portions of 1 N HCl, saturated NaHCO_3 , water, EDTA 0.1 M, water, and brine successively. The organic layer was dried (Na_2SO_4), filtered, and evaporated. The crude product was purified by flash silica gel column chromatography to afford the desired cycloadducts.

General procedure for deacetylation of carbohydrates (method B): The acetylated glycoside was suspended in distilled MeOH, ultrapure water, and ultrapure triethylamine (4:1:1, v/v/v). The mixture was stirred under argon at room temperature for 2 to 4 d. Solvents were evaporated, co-evaporated with toluene, and the resulting white foam was dissolved in ultrapure water (5 mL) and freeze-dried to afford pure hydroxylated glycoconjugates.

Binding studies

Hemagglutination inhibition assays (HIA): Hemagglutination inhibition assays (HIA) were performed in U-shaped 96-well microtitre plates. Rabbit erythrocytes were purchased from Biomérieux and used without further washing. Erythrocytes were diluted to a 4% solution in NaCl (150 mM). PA-IL solutions of 2 mg mL^{-1} were prepared in TRIS-HCl 20 mM (TRIS = tris(hydroxymethyl)aminomethane), NaCl 100 mM, and CaCl_2 100 μM . The hemagglutination unit (HU) was first obtained by the addition of the 4% erythrocyte solution (25 μL) to aliquots (25 μL) of sequential (twofold) lectin dilutions. The mixture was incubated at 25 °C for 60 min. The HU was measured as the minimum lectin concentration required to observe hemagglutination. For the following lectin-inhibition assays, lectin concentrations of 4 HU were used. For PA-IL, this concentration was found to be $8 \mu\text{g mL}^{-1}$. Subsequent inhibition assays were then carried out by the addition of lectin solution (12.5 μL , at the required concentration) to sequential dilutions (25 μL) of glycoclusters, monomer molecules, and controls. These solutions were incubated at 25 °C for 2 h, then 4% erythrocyte solution (12.5 μL) was added, followed by an additional incubation at 25 °C for 30 min. The minimum inhibitory concentration for each molecule was determined for each duplicate.

Determination of lectin concentration by using ELLA: 96-Well microtiter plates (Nunc Maxisorb) were coated with α -PAA-Gal (PAA = polyacrylamide) for PA-IL (Lectinity Holding, Inc.): 100 μL of $5 \mu\text{g mL}^{-1}$ in carbonate buffer, pH 9.6 for 1 h at 37 °C, then blocking at 37 °C for 1 h with 100 μL per well of 3% (w/v) bovine serum albumin (BSA) in phosphate buffer solution (PBS). Lectin solutions (100 μL) were diluted (1:2) starting from 30 $\mu\text{g mL}^{-1}$. After 1 h incubation at 37 °C and three washes with T-PBS (PBS that contained 0.05% Tween 20), horseradish peroxidase (HRP)–streptavidin conjugate (100 μL ; dilution 2:5000; Boehringer–Mannheim) was added and left for 1 h at 37 °C. Coloration was developed by using 100 μL per well of 0.05 M phosphate/citrate buffer that contained *o*-phenylenediamine dihydrochloride (0.4 mg mL^{-1}) and urea hydrogen peroxide (0.4 mg mL^{-1}) (OPD kit, Sigma–Aldrich) for 15 min and stopped with sulfuric acid (50 μL , 30%). Absorbance was then read at 490 nm using a microtiter plate reader (BioRad 680). The concentration of biotinylated lectins was determined by plotting the relative absorbance versus lectin concentration. The concentration that led to the highest response in the linear area was selected as the standard lectin concentration for the subsequent inhibition experiments. The final concentrations were 0.5 $\mu\text{g mL}^{-1}$ for PA-IL.

Determination of inhibition potency (IC_{50}) by using ELLA: ELLAs were conducted using 96-well microtiter plates (Nunc Maxisorb) coated with α -PAA-Gal for PA-IL (Lectinity Holding, Inc.): 100 μL of $5 \mu\text{g mL}^{-1}$ in carbonate buffer, pH 9.6 for 1 h at 37 °C, then blocking at 37 °C for 1 h with 100 μL per well of 3% (w/v) BSA in PBS. Inhibitor solutions (50 μL) were submitted to serial dilutions (1:3) with PBS-BSA 0.3% (w/v). Then, biotinylated lectin solution (50 μL at the appropriate concentration) was added in each well and the plates were incubated for 1 h at 37 °C. After three washings with T-PBS (50 μL , 5 min.), horseradish peroxidase (HRP)–streptavidin conjugate (100 μL ; dilution 2:5000; Boehringer–Mannheim) was added and left for 1 h at 37 °C. After three more washings, coloration was developed using 100 μL per well of 0.05 M phosphate/citrate buffer that contained *o*-phenylenediamine dihydrochloride (0.4 mg mL^{-1}) and urea hydrogen peroxide (0.4 mg mL^{-1}) (OPD kit, Sigma–Aldrich) for 15 min and stopped with sulfuric acid (50 μL , 30%). Absorbance was then read at 490 nm using a microtiter plate reader (BioRad 680) and transformed in inhibition percentage with the help of positive and negative controls. Plots of inhibition percentage versus inhibitor concentration and sigmoidal fitting provided the IC_{50} determination.

Isothermal titration microcalorimetry (ITC): Recombinant lyophilized PA-IL was dissolved in buffer (0.1 M TRIS-HCl, 6 μ M CaCl₂, pH 7.5) and degassed. Protein concentration (between 50 and 120 μ M depending on the ligand affinity) was checked by measurement of optical density by using a theoretical molar extinction coefficient of 28 000. Carbohydrate ligands were dissolved directly into the same buffer, degassed, and placed in the injection syringe (concentration range : monovalent 2–0.7 mM, multivalent 0.2–0.12 mM). ITC was performed using a VP-ITC MicroCalorimeter from MicroCal Incorporated. PA-IL was placed into the 1.4478 mL sample cell, at 25 °C. Titration was performed with 10 μ L injections of carbohydrate ligands every 300 s. Data were fitted using the “one-site model” using MicroCal Origin 7 software according to standard procedures. Fitted data yielded the stoichiometry (n), the association constant (K_A), and the enthalpy of binding (ΔH). Other thermodynamic parameters (i.e., changes in free energy ΔG and entropy ΔS) were calculated from the equation $\Delta G = \Delta H - T\Delta S = -RT \ln K_A$ in which T is the absolute temperature and $R = 8.314 \text{ J mol}^{-1} \text{ K}^{-1}$. Two or three independent titrations were performed for each ligand tested.

Surface plasmon resonance (SPR): SPR inhibition experiments were performed using a Biacore 3000 instrument at 25 °C. Measurements were carried out on two channels with two immobilized sugars: α -L-fucose (channel 1) and α -D-galactose (channel 2). Immobilization of sugars was performed at 25 °C using running buffer (HBS) at 5 μ L min^{−1}. Immobilization on each channel (CM5 Chip) was performed independently as follows. First, the channel was activated by injecting a fresh mixture of EDC/NHS (35 μ L, 420 s). Then a solution of streptavidin (100 μ g mL^{−1} in AcONa pH 5 buffer) was injected (50 μ L, 600 s). The remaining reactive species were quenched by injecting ethanolamine (1 M, 35 μ L, 420 s) into the solution. Finally, a solution of the desired biotinylated-polyacrylamide-sugar (lectinity, 200 μ g mL^{−1}) was coated onto the surface (50 μ L, 600 s) through streptavidin–biotin interaction. This procedure led to 804 RU (resonance units) (fucoside) and 796 RU (galactoside) of immobilized sugars on channels 1 and 2, respectively. Inhibition experiments were performed with the galactosylated channel 2 and plots represent subtracted data (channel 2–channel 1). The running buffer for PA-IL experiments was HEPES 10 mM, NaCl 150 mM, CaCl₂ 10 mM, Tween P20 0.005 %, pH 7.4. Inhibition studies consisted of the injection (150 μ L, 10 μ L min^{−1}, dissociation 120 s) of incubated (> 1 h, RT) mixtures of PA-IL (5 μ M) and various concentrations of inhibitor (twofold cascade dilutions). For each inhibition assay, PA-IL (5 μ M) without inhibitor was injected to observe the full adhesion of the lectin onto the sugar-coated surface (0 % inhibition). The CM5 chip was fully regenerated by successive injections of D-galactose (2 \times 30 μ L, 100 mM in running buffer). Binding was measured as RU over time after blank subtraction, and data were then evaluated using the BIAevaluation Software version 4.1. For IC₅₀ evaluation, the response (R_{eq} –fitted) was considered to be the amount of lectin bound to the carbohydrate-coated surface at equilibrium in the presence of a defined concentration of inhibitor. Inhibition curves were obtained by plotting the percentage of inhibition against the inhibitor concentration (on a logarithmic scale) by using Origin 7.0 software (OriginLab Corp.), and IC₅₀ values were extracted from sigmoidal fit of the inhibition curve.

Molecular modeling: Construction of monovalent references **22**, **3**, **7**, and **10** was performed with Tripos Sybyl 7.3 (Tripos Associates, St. Louis, MO). Atomic partial charges were then calculated (MOPAC/MNDO) for the linker and set up according to Tripos^[69] for the galactose moieties. Linkers and carbohydrates epitopes were connected and the charges were derived and symmetrized to obtain a neutral global charge. The resulting molecule was then energy-minimized by using the conjugate gradient method and TRIPOS Force Field with addition of carbohydrate parameters. This minimization led to 14.4, 14.9, 15.2, and 14.6 kcal mol^{−1} for **22**, **3**, **7**, and **10** respectively. For each compound, the torsion angle Φ was checked to be close to 300° (*exo*-anomeric effect). A systematic search was performed for each compound with 9, 8, 7, and 4 rotatable bonds for **22**, **3**, **7**, and **10**, respectively, and a 20 kcal mol^{−1} energetic cutoff. These systematic searches led to 48 548, 44 324, 26 988, and 7624 reachable conformers for **22**, **3**, **7**, and **10**, respectively. Geometric references and planes were defined for each molecule as follows: S (centroid of all 6 atoms of the carbohydrate ring), T (centroid of all 5 atoms of the triazole

ring), plane T (plane from 3 atoms of the triazole ring), plane N (plane from two extremities of the T centroid normal and the C5 atom of the triazole ring), plane V (plane from centroid S, centroid T, and the endocyclic oxygen of the carbohydrate). Calculations of the geometrical parameters were performed by using these references in the Sybyl spreadsheet.

X-ray crystallography: A crystal suitable for X-ray crystallography was selected and mounted using an Xcalibur κ -geometry diffractometer (Agilent Technologies UK Ltd) equipped with an Eos CCD detector and using MoK α radiation ($\lambda = 0.71073 \text{ \AA}$). Intensities were collected at room temperature by means of the CrysAlisPro software. Reflection indexing, unit-cell parameters refinement, Lorentz-polarization correction, peak integration, and background determination were carried out with the CrysAlisPro software. An analytical absorption correction was applied using the modeled faces of the crystal.^[66] The structures were solved by direct methods with SIR97^[67] and the least-squares refinement on F^2 was achieved with the CRYSTALS software.^[68] All non-hydrogen atoms were refined anisotropically. The hydrogen atoms were all located in a difference map, but those attached to carbon atoms were repositioned geometrically. The hydrogen atoms were initially refined with soft restraints on the bond lengths and angles to regularize their geometry (C–H in the range 0.93 to 0.98 \AA and $U_{iso}(\text{H})$ (in the range 1.2 to 1.5 times U_{eq} of the parent atom), after which the positions were refined with riding constraints. The drawings were achieved with Diamond 3.2 software.^[70] CCDC-845766 (**1e**) contains the supplementary crystallographic data for this paper. These data can be obtained free of charge from The Cambridge Crystallographic Data Centre via www.ccdc.cam.ac.uk/data_request/cif.

Acknowledgements

The authors thank the Université Claude Bernard Lyon 1 and the CNRS for financial support. S.C. thanks the Région Rhône-Alpes (Cluster de Recherche Chimie) and the CNRS (Programme Interdisciplinaire: Chimie pour le Développement Durable) for additional funding. Dr. F. Albrieux, C. Duchamp, and N. Henriques are gratefully acknowledged for mass spectrometry analyses. X-ray crystallographic analyses were performed by Dr. E. Jeanneau at the Centre de Diffraction Henri Longchambon of Université Claude Bernard Lyon 1. Financial help is acknowledged from Vaincre la Mucoviscidose and GDR Pseudomonas. S.V. and A.I. are grateful to financial support from the COST Action CM-1102 MultiGlycoNano. A.I. acknowledges funding from ANR Glycoasterix. M.W. acknowledges the Czech Ministry of Education (MSM0021622413, ME08008). Part of the research has received funding from the European Community's Seventh Framework Programme under grant agreement no. 205872.

- [1] C. R. Bertozzi, L. L. Kiessling, *Science* **2001**, *291*, 2357–2364.
- [2] R. A. Dwek, *Chem. Rev.* **1996**, *96*, 683–720.
- [3] H. Lis, N. Sharon, *Chem. Rev.* **1998**, *98*, 637–674.
- [4] J. C. Paulson, O. Blixt, B. E. Collins, *Nat. Chem. Biol.* **2006**, *2*, 238–248.
- [5] A. Varki, *Glycobiology* **1993**, *3*, 97–130.
- [6] A. Varki, R. D. Cummings, J. D. Esko, H. H. Freeze, P. Stanley, C. R. Bertozzi, G. W. Hart, M. E. Etzler, *Essentials of glycobiology*, Cold Spring Harbor Laboratory Press, Cold Spring Harbor, N. Y., **2009**, p. .
- [7] Y. C. Lee, R. T. Lee, *Acc. Chem. Res.* **1995**, *28*, 321–327.
- [8] J. J. Lundquist, E. J. Toone, *Chem. Rev.* **2002**, *102*, 555–578.
- [9] M. Mammen, S.-K. Choi, G. M. Whitesides, *Angew. Chem.* **1998**, *110*, 2908–2953; *Angew. Chem. Int. Ed.* **1998**, *37*, 2754–2794.
- [10] N. Jayaraman, *Chem. Soc. Rev.* **2009**, *38*, 3463–3483.
- [11] M. Lahmann in *Architectures of Multivalent Glycomimetics for Probing Carbohydrate-Lectin Interactions/Glycoscience and Microbi-*

- al Adhesion*, Vol. 288 (Eds.: T. K. Lindhorst, S. Oscarson), Springer, 2009, pp. 17–65.
- [12] R. J. Pieters, *Org. Biomol. Chem.* **2009**, 7, 2013–2025.
 - [13] N. Sharon, *Biochim. Biophys. Acta Gen. Subj.* **2006**, 1760, 527–537.
 - [14] A. Imberty, Y. M. Chabre, R. Roy, *Chem. Eur. J.* **2008**, 14, 7490–7499.
 - [15] T. K. Dam, C. F. Brewer, *Chem. Rev.* **2002**, 102, 387–430.
 - [16] T. K. Dam, C. F. Brewer, *Biochemistry* **2008**, 47, 8470–8476.
 - [17] O. Sulak, E. Lameignere, M. Wimmerova, A. Imberty in *Specificity and Affinity Studies in Lectin/Carbohydrate Interactions*, Vol. 35 The Royal Society of Chemistry, **2009**, pp. 357–372.
 - [18] M. Touaibia, R. Roy, *Mini-Rev. Med. Chem.* **2007**, 7, 1270–1283.
 - [19] B. Blanchard, A. Nurisso, E. Hollville, C. Tétaud, J. Wiels, M. Pokorná, M. Wimmerová, A. Varrot, A. Imberty, *J. Mol. Biol.* **2008**, 383, 837–853.
 - [20] G. Cioci, E. P. Mitchell, C. Gautier, M. Wimmerova, D. Sudakevitz, S. Pérez, N. Gilboa-Garber, A. Imberty, *FEBS Lett.* **2003**, 555, 297–301.
 - [21] N. Gilboa-Garber, *Methods Enzymol.* **1982**, 83, 378–385.
 - [22] R. U. Kadam, M. Bergmann, M. Hurley, D. Garg, M. Cacciarini, M. A. Swiderska, C. Nativi, M. Sattler, A. R. Smyth, P. Williams, M. Cámara, A. Stocker, T. Darbre, J.-L. Reymond, *Angew. Chem. Int. Ed.* **2011**, 50, 10631–10635.
 - [23] C. Chemani, A. Imberty, S. de Bentzman, P. Pierre, M. Wimmerová, B. P. Guery, K. Faure, *Infect. Immun.* **2009**, 77, 2065–2075.
 - [24] H.-P. Hauber, M. Schulz, A. Pforte, D. Mack, P. Zabel, U. Schumacher, *Int. J. Med. Sci.* **2008**, 5, 371–376.
 - [25] Y. M. Chabre, D. Giguère, B. Blanchard, J. Rodrigue, S. Rocheleau, M. Neault, S. Rauthu, A. Papadopoulos, A. A. Arnold, A. Imberty, R. Roy, *Chem. Eur. J.* **2011**, 17, 6545–6562.
 - [26] S. Cecioni, R. Lalor, B. Blanchard, J.-P. Praly, A. Imberty, S. E. Matthews, S. Vidal, *Chem. Eur. J.* **2009**, 15, 13232–13240.
 - [27] S. Cecioni, S. Faure, U. Darbost, I. Bonnamour, H. Parrot-Lopez, O. Roy, C. Taillefumier, M. Wimmerová, J.-P. Praly, A. Imberty, S. Vidal, *Chem. Eur. J.* **2011**, 17, 2146–2159.
 - [28] J.-F. Nierengarten, J. Iehl, V. Oerthel, M. Holler, B. M. Illescas, A. Munoz, N. Martin, J. Rojo, M. Sanchez-Navarro, S. Cecioni, S. Vidal, K. Buffet, M. Durka, S. P. Vincent, *Chem. Commun.* **2010**, 46, 3860–3862.
 - [29] S. Cecioni, V. Oerthel, J. Iehl, M. Holler, D. Goyard, J.-P. Praly, A. Imberty, J.-F. Nierengarten, S. Vidal, *Chem. Eur. J.* **2011**, 17, 3252–3261.
 - [30] Z. H. Soomro, S. Cecioni, H. Blanchard, J.-P. Praly, A. Imberty, S. Vidal, S. E. Matthews, *Org. Biomol. Chem.* **2011**, 9, 6587–6597.
 - [31] I. Otsuka, B. Blanchard, R. Borsali, A. Imberty, T. Kakuchi, *ChemBioChem* **2010**, 11, 2399–2408.
 - [32] D. Sicard, S. Cecioni, M. Iazykov, Y. Chevolot, S. E. Matthews, J.-P. Praly, E. Souteyrand, A. Imberty, S. Vidal, M. Phaner-Goutorbe, *Chem. Commun.* **2011**, 47, 9483–9485.
 - [33] D. Deniaud, K. Julienne, S. G. Gouin, *Org. Biomol. Chem.* **2011**, 9, 966–979.
 - [34] V. Wittmann, S. Seeberger, *Angew. Chem.* **2004**, 116, 918–921; *Angew. Chem. Int. Ed.* **2004**, 43, 900–903.
 - [35] S. André, Z. Pei, H.-C. Siebert, O. Ramström, H.-J. Gabius, *Bioorg. Med. Chem.* **2006**, 14, 6314–6326.
 - [36] E. Fan, E. A. Merritt, C. L. M. J. Verlinde, W. G. J. Hol, *Curr. Opin. Struct. Biol.* **2000**, 10, 680–686.
 - [37] E. Fan, Z. Zhang, W. E. Minke, Z. Hou, C. L. M. J. Verlinde, W. G. J. Hol, *J. Am. Chem. Soc.* **2000**, 122, 2663–2664.
 - [38] P. I. Kitov, H. Shimizu, S. W. Homans, D. R. Bundle, *J. Am. Chem. Soc.* **2003**, 125, 3284–3294.
 - [39] E. A. Merritt, Z. Zhang, J. C. Pickens, M. Ahn, W. G. J. Hol, E. Fan, *J. Am. Chem. Soc.* **2002**, 124, 8818–8824.
 - [40] D. Schwefel, C. Maierhofer, J. G. Beck, S. Seeberger, K. Diederichs, H. M. Möller, W. Welte, V. Wittmann, *J. Am. Chem. Soc.* **2010**, 132, 8704–8719.
 - [41] Z. Zhang, E. A. Merritt, M. Ahn, C. Roach, Z. Hou, C. L. M. J. Verlinde, W. G. J. Hol, E. Fan, *J. Am. Chem. Soc.* **2002**, 124, 12991–12998.
 - [42] P. I. Kitov, J. M. Sadowska, G. Mulvey, G. D. Armstrong, H. Ling, N. S. Pannu, R. J. Read, D. R. Bundle, *Nature* **2000**, 403, 669–672.
 - [43] S. André, B. Liu, H.-J. Gabius, R. Roy, *Org. Biomol. Chem.* **2003**, 1, 3909–3916.
 - [44] C. Bouillon, A. Meyer, S. Vidal, A. Jochum, Y. Chevolot, J.-P. Cloarec, J.-P. Praly, J.-J. Vasseur, F. Morvan, *J. Org. Chem.* **2006**, 71, 4700–4702.
 - [45] Y. Chevolot, C. Bouillon, S. Vidal, F. Morvan, A. Meyer, J. P. Cloarec, A. Jochum, J. P. Praly, J. J. Vasseur, E. Souteyrand, *Angew. Chem.* **2007**, 119, 2450–2454; *Angew. Chem. Int. Ed.* **2007**, 46, 2398–2402.
 - [46] J. Li, S. Zacharek, X. Chen, J. Wang, W. Zhang, A. Janczuk, P. G. Wang, *Bioorg. Med. Chem.* **1999**, 7, 1549–1558.
 - [47] F. Morvan, A. Meyer, A. Jochum, C. Sabin, Y. Chevolot, A. Imberty, J.-P. Praly, J.-J. Vasseur, E. Souteyrand, S. Vidal, *Bioconjugate Chem.* **2007**, 18, 1637–1643.
 - [48] N. Nagahori, S.-I. Nishimura, *Biomacromolecules* **2001**, 2, 22–24.
 - [49] Z. Szurmai, L. Szabo, A. Liptak, *Acta Chim. Hung.* **1989**, 126, 259–269.
 - [50] C.-S. Tsai, T.-B. Yu, C.-T. Chen, *Chem. Commun.* **2005**, 4273–4275.
 - [51] G. Fischer, *Chem. Soc. Rev.* **2000**, 29, 119–127.
 - [52] N. Garber, U. Guempel, A. Belz, N. Gilboa-Garber, R. J. Doyle, *Biochim. Biophys. Acta Gen. Subj.* **1992**, 1116, 331–333.
 - [53] J. L. Xue, S. Cecioni, L. He, S. Vidal, J.-P. Praly, *Carbohydr. Res.* **2009**, 344, 1646–1653.
 - [54] S. Cecioni, M. Almant, J.-P. Praly, S. Vidal in *Synthesis of Azido-Functionalized Carbohydrates for the Design of Glycoconjugates*, Vol. 1 (Ed. P. Kováč), CRC Press, **2012**, pp. 175–180.
 - [55] V. I. Rostovtsev, L. G. Green, V. V. Fokin, K. B. Sharpless, *Angew. Chem.* **2002**, 114, 2708–2711; *Angew. Chem. Int. Ed.* **2002**, 41, 2596–2599.
 - [56] C. W. Tornøe, C. Christensen, M. Meldal, *J. Org. Chem.* **2002**, 67, 3057–3064.
 - [57] M. Meldal, C. W. Tornøe, *Chem. Rev.* **2008**, 108, 2952–3015.
 - [58] F. Perez-Balderas, J. Morales-Sanfrutos, F. Hernandez-Mateo, J. Isac-García, F. Santoyo-Gonzalez, *Eur. J. Org. Chem.* **2009**, 2441–2453.
 - [59] Y. Liu, C.-F. Ke, H.-Y. Zhang, J. Cui, F. Ding, *J. Am. Chem. Soc.* **2008**, 130, 600–605.
 - [60] W. B. Turnbull, A. H. Daranas, *J. Am. Chem. Soc.* **2003**, 125, 14859–14866.
 - [61] A. Imberty, S. Pérez, M. Hricovini, R. N. Shah, J. P. Carver, *Int. J. Biol. Macromol.* **1993**, 15, 17–23.
 - [62] K. N. Houk, A. G. Leach, S. P. Kim, X. Zhang, *Angew. Chem.* **2003**, 115, 5020–5046; *Angew. Chem. Int. Ed.* **2003**, 42, 4872–4897.
 - [63] L. Liu, Q.-X. Guo, *Chem. Rev.* **2001**, 101, 673–696.
 - [64] E. Grunwald, C. Steel, *J. Am. Chem. Soc.* **1995**, 117, 5687–5692.
 - [65] A. Cornish-Bowden, *J. Biosci.* **2002**, 27, 121–126.
 - [66] R. C. Clark, J. S. Reid, *Acta Crystallogr. Sect. A* **1995**, 51, 887–897.
 - [67] A. Altomare, M. C. Burla, M. Camalli, G. L. Cascarano, C. Giacovazzo, A. Guagliardi, A. G. G. Moliterni, G. Polidori, R. Spagna, *J. Appl. Crystallogr.* **1999**, 32, 115–119.
 - [68] P. W. Betteridge, J. R. Carruthers, R. I. Cooper, K. Prout, D. J. Watkin, *J. Appl. Crystallogr.* **2003**, 36, 1487.
 - [69] A. Imberty, E. Bettler, M. Karababa, K. Mazeau, P. Petrova, S. Pérez in *Building Sugars: The Sweet Part of Structural Biology* (Eds.: M. Vijayan, N. Yathindra, A. S. Kolaskar), Indian Academy of Sciences and Universities Press, Hyderabad, **1999**, pp. 392–409.
 - [70] Diamond version 3.2, M. Berndt, K. Brandenburg, H. Putz, 1999, Bonn (Germany), Crystal Impact GbR.

Received: January 2, 2012
Published online: April 4, 2012